Eur. Phys. J. A (2013) **49**: 156
DOI 10.1140/epja/i2013-13156-x

THE EUROPEAN PHYSICAL JOURNAL A

Special Article – Tools for Experiment and Theory

High-accuracy determination of the neutron flux at n_TOF

M. Barbagallo[1a], C. Guerrero[2], A. Tsinganis[2,3], D. Tarrío[4], S. Altstadt[5], S. Andriamonje[2], J. Andrzejewski[6], L. Audouin[7], V. Bécares[8], F. Bečvář[9], F. Belloni[10], E. Berthoumieux[10,2], J. Billowes[11], V. Boccone[2], D. Bosnar[12], M. Brugger[2], M. Calviani[2], F. Calviño[13], D. Cano-Ott[8], C. Carrapiço[14], F. Cerutti[2], E. Chiaveri[10,2], M. Chin[2], N. Colonna[1], G. Cortés[13], M.A. Cortés-Giraldo[15], M. Diakaki[3], C. Domingo-Pardo[16], I. Duran[4], R. Dressler[17], N. Dzysiuk[18], C. Eleftheriadis[19], A. Ferrari[2], K. Fraval[10], S. Ganesan[20], A.R. García[8], G. Giubrone[16], K. Göbel[5], M.B. Gómez-Hornillos[13], I.F. Gonçalves[14], E. González-Romero[8], E. Griesmayer[21], F. Gunsing[10], P. Gurusamy[20], A. Hernández-Prieto[2,13], D.G. Jenkins[22], E. Jericha[21], Y. Kadi[2], F. Käppeler[23], D. Karadimos[3], N. Kivel[17], P. Koehler[24], M. Kokkoris[3], M. Krtička[9], J. Kroll[9], C. Lampoudis[10], C. Langer[5], E. Leal-Cidoncha[4], C. Lederer[5,25], H. Leeb[21], L.S. Leong[7], R. Losito[2], A. Manousos[19], J. Marganiec[6], T. Martínez[8], C. Massimi[26], P.F. Mastinu[18], M. Mastromarco[1], M. Meaze[1], E. Mendoza[8], A. Mengoni[27], P.M. Milazzo[28], F. Mingrone[26], M. Mirea[29], W. Mondalaers[30], T. Papaevangelou[10], C. Paradela[4], A. Pavlik[25], J. Perkowski[6], A. Plompen[30], J. Praena[15], J.M. Quesada[15], T. Rauscher[31], R. Reifarth[5], A. Riego[13], F. Roman[2,29], C. Rubbia[2,32], M. Sabate-Gilarte[15], R. Sarmento[14], A. Saxena[20], P. Schillebeeckx[30], S. Schmidt[5], D. Schumann[17], P. Steinegger[17], G. Tagliente[1], J.L. Tain[16], L. Tassan-Got[7], S. Valenta[9], G. Vannini[26], V. Variale[1], P. Vaz[14], A. Ventura[27], R. Versaci[2], M.J. Vermeulen[22], V. Vlachoudis[2], R. Vlastou[3], A. Wallner[25], T. Ware[11], M. Weigand[5], C. Weiß[5,2], T. Wright[11], and P. Žugec[12]

[1] INFN, Sezione di Bari, V. Orabona 4, 70125 Bari, Italy
[2] European Organization for Nuclear Research (CERN), Geneva, Switzerland
[3] National Technical University of Athens (NTUA), Greece
[4] Universidade de Santiago de Compostela, Spain
[5] Johann-Wolfgang-Goethe Universität, Frankfurt, Germany
[6] Uniwersytet Łódzki, Lodz, Poland
[7] Centre National de la Recherche Scientifique/IN2P3 - IPN, Orsay, France
[8] Centro de Investigaciones Energeticas Medioambientales y Tecnológicas (CIEMAT), Madrid, Spain
[9] Charles University, Prague, Czech Republic
[10] Commissariatà l'Energie Atomique (CEA) Saclay - Irfu, Gif-sur-Yvette, France
[11] University of Manchester, Oxford Road, Manchester, UK
[12] Department of Physics, Faculty of Science, University of Zagreb, Croatia
[13] Universitat Politecnica de Catalunya, Barcelona, Spain
[14] Instituto Tecnológico e Nuclear, Instituto Superior Técnico, Universidade Técnica de Lisboa, Lisboa, Portugal
[15] Universidad de Sevilla, Spain
[16] Instituto de Física Corpuscular, CSIC-Universidad de Valencia, Spain
[17] Paul Scherrer Institut, Villigen PSI, Switzerland
[18] INFN, Laboratori Nazionali di Legnaro, Italy
[19] Aristotle University of Thessaloniki, Thessaloniki, Greece
[20] Bhabha Atomic Research Centre (BARC), Mumbai, India
[21] Atominstitut, Technische Universität Wien, Austria
[22] University of York, Heslington, York, UK
[23] Karlsruhe Institute of Technology, Campus Nord, Institut für Kernphysik, Karlsruhe, Germany
[24] Oak Ridge National Laboratory (ORNL), Oak Ridge, TN 37831, USA
[25] University of Vienna, Faculty of Physics, Austria
[26] Dipartimento di Fisica, Università di Bologna, and INFN, Sezione di Bologna, Italy
[27] Agenzia nazionale per le nuove tecnologie, l'energia e lo sviluppo economico sostenibile (ENEA), Bologna, Italy
[28] INFN, Sezione di Trieste, Italy
[29] Horia Hulubei National Institute of Physics and Nuclear Engineering - IFIN HH, Bucharest - Magurele, Romania
[30] European Commission JRC, Institute for Reference Materials and Measurements, Retieseweg 111, B-2440 Geel, Belgium
[31] Department of Physics and Astronomy - University of Basel, Basel, Switzerland
[32] Laboratori Nazionali del Gran Sasso dell'INFN, Assergi (AQ), Italy

Received: 16 May 2013 / Revised: 1 November 2013
Published online: 18 December 2013 –
Communicated by P. Woods

Abstract. The neutron flux of the n_TOF facility at CERN was measured, after installation of the new spallation target, with four different systems based on three neutron-converting reactions, which represent accepted cross sections standards in different energy regions. A careful comparison and combination of the different measurements allowed us to reach an unprecedented accuracy on the energy dependence of the neutron flux in the very wide range (thermal to 1 GeV) that characterizes the n_TOF neutron beam. This is a pre-requisite for the high accuracy of cross section measurements at n_TOF. An unexpected anomaly in the neutron-induced fission cross section of ^{235}U is observed in the energy region between 10 and 30 keV, hinting at a possible overestimation of this important cross section, well above currently assigned uncertainties.

1 Introduction

The neutron time-of-flight facility n_TOF was built at CERN more than ten years ago with the aim of providing new and accurate cross sections for neutron-induced reactions of interest for fundamental and applied nuclear science [1]. The experimental activity is focused mostly on the measurements of neutron capture reactions involved in stellar nucleosynthesis [2,3], as well as on capture and fission reactions relevant to nuclear technology [4,5]. Relative to other time-of-flight facilities, the n_TOF neutron beam in the current experimental area, located at 185 m from the spallation target, is characterized by a unique combination of high luminosity, wide energy range, high resolution and low duty cycle.

After the first four years of operation (n_TOF-Phase1), the spallation target had to be replaced, due to some corrosion caused by insufficient cooling. In 2008, a new spallation target was installed together with a new cooling/moderator assembly, and a new experimental campaign was started (n_TOF-Phase2) [6]. Contrary to the first assembly, for which the cooling water acted also as moderator, the moderator system of the new design was decoupled from the cooling circuit to allow the use of different materials. At present, cooling is ensured by a layer 1 cm in thickness, providing also some moderation of the neutron spectrum. Further moderation is ensured by a 4 cm thick layer of another liquid. Apart from demineralized water, borated or heavy water can be used, to minimize radiative neutron capture on hydrogen and consequent production of 2.2 MeV γ-rays, responsible for additional background in capture cross section measurements in the keV neutron energy region.

After installation of the new spallation target and of the upgraded cooling and moderation system, and before the start of a new experimental campaign, a series of measurements was performed with the aim of characterizing the new neutron beam. An overview of the measurements and related results has already been published [7]. One of the most important characteristics of the new beam, which has to be determined with high accuracy, is the neutron flux. The knowledge of this quantity, or more specifically of the total number of neutrons impinging on the sample during the measurement as a function of neutron energy, is a fundamental prerequisite for high-accuracy cross section measurements. To this end, a large effort has been devoted at n_TOF to minimize possible sources of uncertainty, both systematic and statistical, in particular with respect to the energy dependence of the neutron flux. We remark that the requirement of a high accuracy on the absolute value of the flux is not crucial, since in all cross section measurements an absolute normalization can be determined in a particular energy range with respect to a standard reaction (for example, the ^{197}Au for capture cross section measurements and the ^{235}U(n, f) for fission).

In this paper, the results of the neutron flux measurements performed during n_TOF-Phase2 are presented and discussed. The measurements were performed for the two cooling/moderator configurations used so far: i) a 5 cm layer of demineralized water and, ii) a combination of 1 cm layer of demineralised water plus a 4 cm layer of borated water (H_2O + 1.28%H_3BO_3, fraction in mass).

To minimize systematic uncertainties related to the experimental technique, three different neutron converting reactions were used, in combination with four different detection systems, some of which were permanently installed in the experimental area in order to monitor the beam stability and determine the neutron fluence in each measurement.

The results of the various measurements were compared and combined in order to identify and minimize systematic uncertainties. While the goal of a high-accuracy neutron flux was achieved in most of the neutron energy range of the n_TOF neutron beam, the analysis revealed an unexpected possible anomaly in the fission cross section of ^{235}U in the neutron energy range between 10 and 30 keV, calling for a further, dedicated investigation.

The paper is organized as follows: the experimental setup is described in sect. 2, while the data analysis for the various detectors/reactions are discussed in detail in sect. 3. The final results including systematic uncertainties are given in sect. 4, together with a discussion of the possible anomaly on the fission cross section of ^{235}U.

2 The experimental setup

In cross section measurements, in particular for neutron capture reactions, it is fundamental to know the total number of neutrons impinging on the sample during the whole measurement. This quantity can be obtained from the flux, *i.e.* the number of neutrons per unit time and unit surface, integrated over the sample surface and over the duration of the measurement. At n_TOF, where the spatial profile of the neutron beam is not uniform and neutrons are delivered in bunches at a very low repetition

[a] e-mail: massimo.barbagallo@ba.infn.it

Table 1. Reactions exploited at n_TOF to characterize the flux.

Reaction	Standard energy range
^{6}Li(n,α)	0.0253 eV to 1 MeV
^{10}B(n,α)	0.0253 eV to 1 MeV
^{235}U(n,f)	0.0253 eV and 0.15 MeV to 200 MeV

rate (< 0.8 Hz), it is more convenient to consider the total number of neutrons in a bunch. For simplicity, in this work we will call this quantity *the flux* (although a more correct definition would be neutron intensity). Similarly, *the fluence* will be used hereafter to indicate the time-integrated flux defined above.

Neutron flux measurements are performed by means of neutron-converting reactions. In table 1 the reactions used for the characterization of the n_TOF beam are listed. Together with the advantage of a high cross section at thermal neutron energy, these reactions are characterized by a cross section of very high accuracy in some particular energy regions, where these reactions are considered as standards [8,9].

Because each reaction represents a cross section standard in a limited energy range (indicated in table 1), a single reaction is not sufficient to cover the wide energy range of the n_TOF neutron beam, which extends from thermal energy to approximately 1 GeV, and a combination of different reactions has to be used instead. It is important to remark that the cross section standards mentioned above overlap in some energy regions, so that by comparing and combining the results it is possible to identify and correct for possible systematic uncertainties affecting the detection systems and/or the analysis procedure, thus substantially improving the accuracy of the extracted neutron flux.

In combination with these different reactions, various detectors were also used, based on different working principles, so as to minimize systematic effects related to the detector efficiency and other experimental effects. The following systems were used: i) a solid state detection system equipped with ^{6}Li converter (the silicon monitor device, or SiMon [10]); ii) a Micromegas gas detector (MGAS) [11, 12] equipped with ^{10}B and ^{235}U converters; iii) a calibrated fission chamber from Physikalisch Technische Bundesanstalt (PTB) [13], equipped with a ^{235}U converter; iv) a set of Parallel Plate Avalanche Counters (PPAC) [14, 15] equipped with a ^{235}U converter. The first three systems were inserted in the beam, as sketched in fig. 1 and data were taken with the so-called "capture" collimator, *i.e.* a collimator with an aperture of 1.8 cm located immediately before the experimental area and used in capture cross section measurements. The PPAC measurements were performed separately with a collimator with an aperture of 8 cm, used for fission measurements.

In brief, the SiMon detector consists of a Mylar foil 5 cm in diameter, with a 300 μg/cm^2 deposit of pure ^{6}Li, centered in the beam and surrounded by an array of four silicon detectors outside the beam in forward direction.

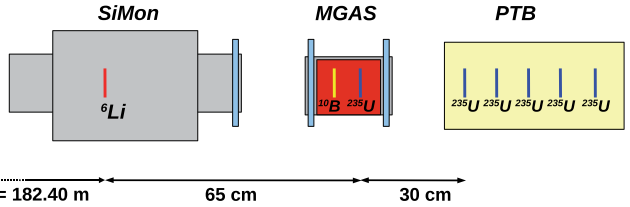

Fig. 1. Schematic view of the detector placements in the flight path. The distance between the spallation target and the SiMon detector is also indicated ($L = 182.40$ m), together with the relative distances between the various detectors.

This system which records the tritons and alpha particles emitted in ^{6}Li$(n,\alpha)t$ reaction (Q-value 4.78 MeV) has been used since 2001 to monitor the neutron flux during capture cross section measurements.

MicroMegas is a family of gaseous detectors, initially developed for high-energy experiments, characterized by low noise, high radiation resistance and low mass. For several years, they have been used at n_TOF for measuring the neutron flux, the spatial beam profile and, more recently, for measurements of neutron-induced fission cross sections. A new version of the Micromegas detector, based on the Micro Bulk technology [16], is currently being used at n_TOF, where further improvements have been introduced leading to an essentially transparent detector. The detector for the flux measurement consists of a gas volume separated by a thin micro-mesh into a 5 mm wide drift region with an electric field of ~ 1 kV/cm and a narrow amplification gap 25 to 50 μm in thickness with an electric field of ≥ 10 kV/cm. All electrodes are 10 cm in diameter.

In the MGAS neutron detection is achieved by means of ^{10}B and ^{235}U converters deposited on the cathode, each 70 mm in diameter. The first converter consists of a 12 μm thick coppered Kapton foil with 0.6 μm $^{10}B_4C$ deposit; the other one is a 1.5 μm thick aluminized Mylar foil with 1 mg of 99.94% enriched ^{235}U deposit. Hereafter we will refer to the two detectors as MGAS(^{10}B) and MGAS(^{235}U), respectively. The MGAS detectors are mounted inside a cylindrical aluminum chamber 15 cm in diameter, in which a mixture of Ar, 10% CF_4 and 2% iC_4H_{10} is circulated at atmospheric pressure. The entrance and exit windows for the neutron beam are made of Kapton because of its resistance against radiation damage and its low interaction cross section with neutrons.

The third system used for the measurement is a calibrated ionization chamber from Physikalisch-Technische Bundesanstalt [13]. The chamber is equipped with ^{235}U deposits on 76 mm in diameter and about 500 μg/cm^2 in thickness on both sides of five platinum electrodes. In total, 201.4(5) mg of ^{235}U are used. The detector, which is very well characterized in terms of detection efficiency and uniformity of the fissile deposit, is considered a reference in the field of metrology. Accordingly, it is perfectly suited for the measurement of the absolute neutron flux as well as for its energy dependence in the energy range between 0.15 and 200 MeV, where the ^{235}U(n,f) cross section is an accepted standard.

Finally, a set of Parallel Plate Avalanche Counters with a ^{235}U converter were used. The detector is described in detail in refs. [14,15]. The PPAC used have a central anode flanked by two cathodes. A low-pressure gas fills the 3 mm gaps between the aluminized Mylar electrodes (1.5 μm thick). The ^{235}U sample used in the neutron flux measurement was 8 cm in diameter and 240 μg/cm^2 in thickness.

After preamplification, the data are directly processed with the standard n_TOF Data Acquisition Systems [17], based on flash-ADCs recording the full wave form of the signals with a sampling rate up to 1 GS/s, 8 bit resolution and 8 MBytes on-board memory. For all four detectors, data were collected for a time of flight of 80 ms, corresponding to close to thermal neutron energy ($\sim$ 30 meV). Each signal was reconstructed with a dedicated routine in order to extract its amplitude, area, and time information. The neutron flux measurements were performed as part of the commissioning of the new spallation target, in 2009, before the start of the second experimental campaign at n_TOF. In this first measurement, normal water was used as moderator. The measurements were then repeated at the beginning of 2010 after changing the moderator to borated water, and again in 2011, to check for the stability of the moderator system.

3 Data analysis

The neutron flux $\Phi(E_n)$ is extracted from the measurement based on a given neutron-converting reaction, according to the following relation:

$$\Phi(E_n) = \frac{C(E_n) - B(E_n)}{\varepsilon(E_n) \cdot \left(1 - e^{-n \cdot \sigma_t(E_n)}\right) \frac{\sigma_r(E_n)}{\sigma_t(E_n)}}, \qquad (1)$$

where C is the total number of counts per bunch (defined later), B the background contribution and n is the areal density (atoms/barn) of the deposit used for neutron conversion. The quantities σ_r and σ_t are, respectively, the reaction and total cross section for the isotope used as neutron converter. In this work the evaluated cross section from the ENDF-B/VII.1 library were used for ^{6}Li, ^{10}B and ^{235}U. Finally, ε is the efficiency for detecting the product of the neutron interaction. All the above mentioned quantities, except n, are functions of the neutron energy E_n. For this reason, the uncertainty on the energy dependence of the flux depends, for each detector, on the uncertainty on the reaction cross sections as well as on the variation with energy of the efficiency correction. For each detector, the uncertainty related to these quantities will be discussed separately. On the other hand, since it is not crucial to determine the absolute value with high accuracy, the uncertainty on the areal density of the neutron-converting deposits does not contribute significantly to the error budget, except, to some extent, for the PTB detector used for normalization. A similar argument applies to tha absolute value of the efficiency correction. Finally, it is important to remark that, in all but the PTB case, the uncertainty on the total cross section propagates only for a very small fraction to the final uncertainty, being $n\sigma_t(E_n) \ll 1$ for both SiMon and MGAS cases. For this reason, it can be safely neglected in the uncertainty determination.

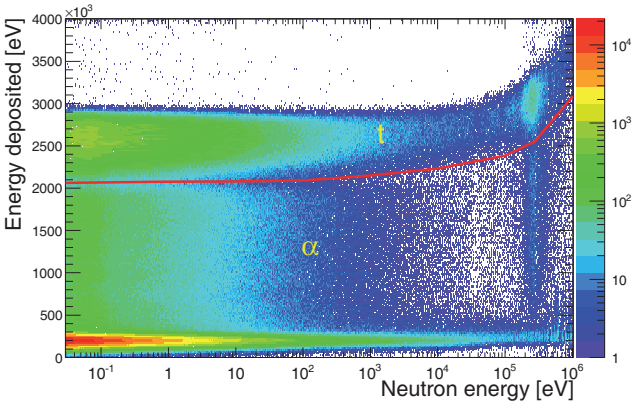

Fig. 2. Energy deposition in SiMon as a function of neutron energy. The red solid curve represents the 2-dimensional threshold condition used in the analysis to select tritons.

As already mentioned, it is convenient to express the neutron flux as the total number of neutrons in a reference pulse corresponding to $7 \cdot 10^{12}$ protons (this number represents the typical proton intensity for a dedicated pulse delivered by the PS to the n_TOF experiment). Therefore, in eq. (1) the total number of counts recorded in the measurement is divided by the total number of incident protons and multiplied by $7 \cdot 10^{12}$. The neutron energy calibration in all cases was performed by analysing the lowest lying resonances in the ^{235}U fission data, discussed later, with a correction on the flight path equal to the relative distance between each detector and the MGAS(^{235}U) one; the neutron energy calibration was double checked with the same procedure using ^{235}U samples in PTB detector.

3.1 The SiMon detector

The analysis of the SiMon data is based on the selection of tritons emitted in the ^{6}Li$(n,\alpha)t$ reaction. For the Li foil used, the triton peak is well defined and separated from the α-particles, which instead are not completely resolved from the electronic noise due to their energy loss in the foil, in particular for larger emission angles. Although the Q-value of the reaction is quite large (4.8 MeV), the triton energy remains constant only for neutron energies below approximately 100 keV, drifting towards higher values with increasing neutron energy. Therefore, a two-dimensional condition has to be applied, in order to select only the triton peak. Figure 2 shows the 2D plot of the energy deposited in the SiMon *versus* neutron energy for all four silicon detectors (the energy deposited in each detector was calibrated using the triton peak itself). The kinematic effects with increasing neutron energy are evident. The solid red line in the figure represents the 2-dimensional condition used in the analysis to select only tritons. A possible variation of the efficiency with neutron energy may be

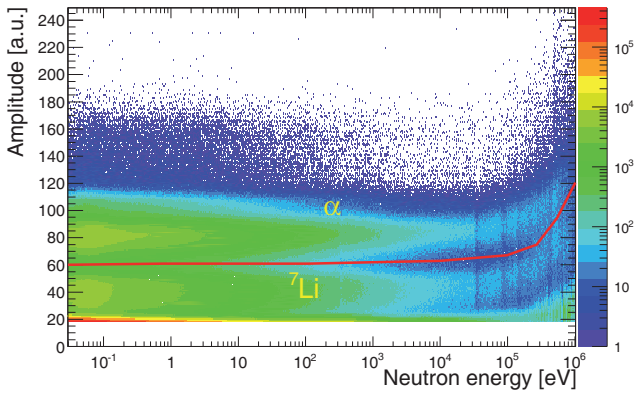

Fig. 3. Amplitude distribution in MGAS(^{10}B) detector as a function of neutron energy. The red solid curve represents the 2-dimensional condition used in the analysis to select α-particles.

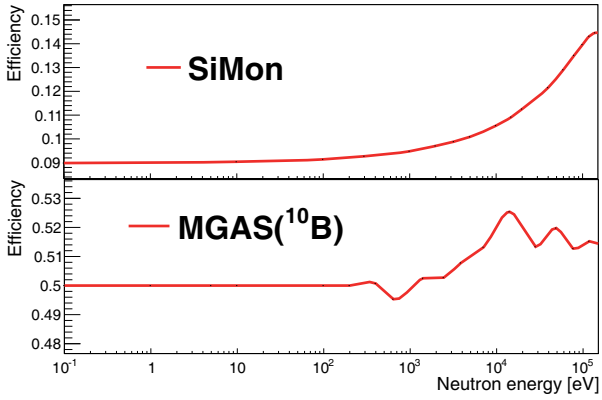

Fig. 4. Efficiency for the detection of tritons from the ^{6}Li(n,α) reaction (top panel) and for α-particles from the ^{10}B$(n,\alpha)^7$Li reaction in the MGAS(^{10}B) detector (bottom panel).

related to the bleed-through of α-particles above threshold and, conversely, to the loss of tritons below threshold. This effect has been checked with the simulations, revealing that with the applied 2D condition, both effects are small and, mostly importantly, their variation with energy is well below the declared uncertainty.

As discussed in [10], Geant4 [18] simulations have shown that the efficiency of the SiMon detector is constant below 1 keV neutron energy ($\sim$ 9%). At higher energies, the forward peaked angular distribution of tritons causes an increase of the efficiency to values between 12 and 15%, as shown in top panel in fig. 4. Although ^{6}Li(n,α) cross section is known with an accuracy of 1%, it is important to note that the angular distribution of reaction products is not so well characterized. Therefore the simulated efficiency above a few keV is affected by a larger uncertainty, around 3%, than in the low energy region.

3.2 The MicroMegas detector with ^{10}B converter

The determination of the flux with the MGAS(^{10}B) relies on the use of a ^{10}B deposit as neutron converter. The ^{10}B$(n,\alpha)^7$Li reaction has two exit channels, with the residue left in the ground state or in the first excited state, decaying to the ground state with the emission of a 478 keV γ-ray. In this second channel, characterized by a branching ratio of 94% for thermal neutrons, α-particles are emitted with 1.47 MeV kinetic energy, while 0.84 MeV are carried out by the ^{7}Li nucleus. Both products deposit their full kinetic energy in the drift volume of the MicroMegas detector. Similarly to the SiMon case, to extract the neutron flux, a condition has to be used in the analysis to select only α-particles, which are well above threshold and not affected by electronic noise. To this end, a 2D cut on the deposited energy was set as a function of the neutron energy, since the energy available for the reaction products increases with neutron energy, as shown in fig. 3.

The efficiency for the detection of α-particles emitted in both exit channels of the ^{10}B(n,α) reaction was calculated taking into account the angular distribution of reaction products reported in ref. [19]. The bottom panel in fig. 4 shows the result of the calculation. As in the case of SiMon, the efficiency of the MGAS(^{10}B) detector is constant at low neutron energies, but starts changing above a few keV, due to a backward/forward anisotropy in the angular distribution of the emitted α-particles. It is important to note that, in this case as well, it is not necessary to determine with high accuracy the value of the efficiency, since the results are normalized to the PTB calibrated fission chamber. On the contrary, the energy dependence of the efficiency is important, as it affects the shape of the neutron flux.

Since the MGAS(^{10}B) is positioned in the neutron beam after the SiMon detector a correction for the attenuation of the neutron beam in the lithium converter has been considered. Such a correction is of the order of a few percent close to thermal neutron energy, but negligible at all other energies. Due to the small value of the correction, the related uncertainty, associated with the well known total cross section of ^{6}Li and to the areal densities of the mylar and ^{6}Li deposit, known to better than 10%, is well below 1%, and can be neglected in the uncertainty budget. We have also verified the effect of the bleed-through of ^{7}Li particles above threshold and the loss of α-particles below threshold. To this purpose, detailed Monte Carlo simulations of the energy loss in the deposit and in the gas volume have been performed. The first effect is negligible, being less than a percent in the whole energy region. On the contrary, the loss of efficiency due to α-particles falling below the threshold is around 14%, but it remains constant as a function of neutron energy, within 1% percent, all the way up to 100 keV.

3.3 The MicroMegas detector with ^{235}U converter

The analysis of the MGAS(^{235}U) relies on the selection of one of the fission fragments (FF). The Q-value of neutron-induced fission of ^{235}U is very large, thus allowing in principle to well separate signals produced by fission fragments

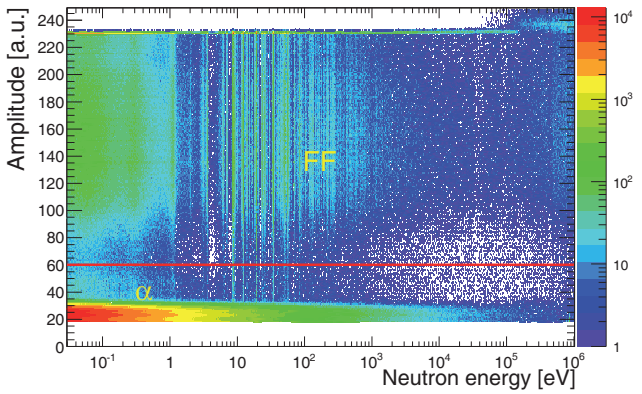

Fig. 5. Pulse amplitude spectrum recorded with the MGAS(^{235}U) detector as a function of neutron energy. The α-particles from the natural radioactivity of the sample are visible below channels 40–50. The counts around channel 230 correspond to a saturation of the 8 bits digitizers.

from spurious ones due to electronic noise or other sources of background (in particular α-particles from the natural radioactivity of this isotope). Figure 5 shows the amplitude distribution of the signals in the detector as a function of neutron energy, indicating that in this case a cut constant in energy is sufficient to discriminate fission fragments from the background. In this respect a threshold at channel 60, illustrated in fig. 5, was chosen to ensure maximum efficiency, which has been determined to 94% by simulation of the energy loss of the fragments in the uranium deposit and in the gas. The efficiency is constant up to a few MeV, due to the absence of angular distribution effects. When extracting the flux, as in the case of the MGAS(^{10}B), the transmission through the upstream converters has been taken into account. Specifically, the attenuation in the ^{6}Li and ^{10}B deposits has to be considered, due to their very high cross section, while the effect of electrodes and vacuum windows is negligible.

The MGAS(^{235}U) detector was also used for neutron energy calibration. As described in detail in [7,20], the neutron energy is reconstructed from the time of flight, provided that the effective flight path length is accurately known (this includes, together with the geometrical distance between the spallation target and the detector, an additional distance related to the moderation process inside the target/moderation assembly). The effective flight path length is experimentally determined by a best fit of the measured resonance energies to the recommended values extracted in this case from the ENDF-B/VII.1 library. An additional energy-dependent correction has to be considered for the effective flight path length, which becomes important in particular above a few hundred keV. The correction has been estimated from simulations and included in the analysis.

Once the effective flight path is determined for the MGAS(^{235}U), the flight base for all other detectors is easily determined by their geometrical distance from the MGAS(^{235}U) detector itself.

Table 2. Summary of the relative (%) systematic uncertainties associated with the measurement of the flux performed with PTB detector near thermal energy and between 100 keV and 10 MeV.

	$E_n = 30$ meV	100 keV $< E_n <$ 10 MeV
Cross section	0.5%	$\leq$ 1%
Sample mass	0.7%	0.7%
Beam attenuation	$\sim$ 0.8%	$\sim$ 1.%
Efficiency	1.5%	1.5%
FF ang. distr.	negligible	negligible
Dead time	negligible	$\leq$ 0.5%
Total	1.9%	$\leq$ 2.3%

3.4 The PTB fission chamber

The analysis of the data taken with the PTB chamber relies on the selection of fission fragments. Based on the values reported in [13], the detection efficiency accounting only for the loss of fission fragments was assumed to be 93.3% if the threshold is chosen at 45% of the maximum of the distribution. The efficiency is constant in the entire energy range where the PTB detector has been used. Apart from the efficiency, however, corrections have to be applied for the neutron capture and scattering (including backscattering) in the Ta windows and electrodes, as well as in the Pt backings used for the ^{235}U deposit. An accurate estimate of these effects can only be performed by means of Monte Carlo simulations. To this end, the complete set-up was implemented in MCNPX [21] and a simulation using a white neutron beam with energies between 30 meV and 10 MeV was carried out. The correction at 30 meV amounts to $\sim$ 15%, while above a few keV it is of the order of a few percent on average (depending locally on the presence of narrow and sizable resonances in the structural materials). The uncertainty related to these corrections is, typically, small. In particular, considering the uncertainty on the total cross section of Ta and Pt, of 3.5% and 3.3%, respectively, the corrections for capture and scattering in the Pt backing and in the Ta windows and electrodes lead to a maximum uncertainty on the extracted value of the flux of 0.6%, at the lowest energy ($\sim$ 30 meV). Combined with the uncertainty on the fission cross section of ^{235}U (0.5% up to almost 1 eV) and with the uncertainty on the areal density of the^{235}U deposit (0.7%), the overall uncertainty on the absolute value of the extracted flux is 1.9%, while considering only the energy-dependent terms it is below 1% all the way up to 1 eV. As for all other detectors, the neutron flux extracted from the PTB chamber has been corrected for the attenuation of the beam in the various deposits, backings, electrodes and windows upstream of the chamber. In all cases, the uncertainty on such a correction is below 1%. The uncertainties budget is reported in table 2, for the energy ranges where the PTB detector has been used.

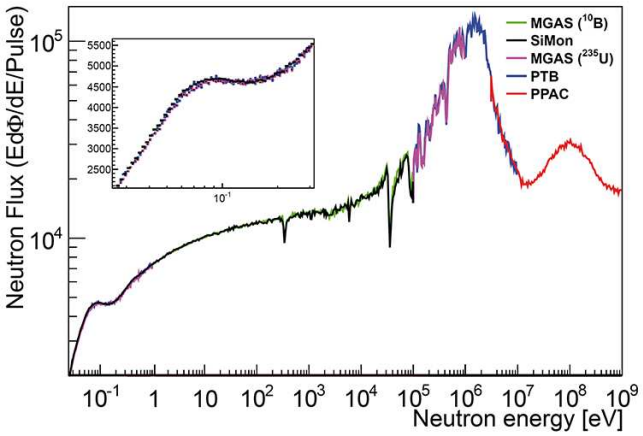

Fig. 6. Overall comparison for flux extracted by SiMon, MGAS(^{10}B), MGAS(^{235}U), PTB and PPAC detectors. All results have been normalized close to thermal energy to the value provided by the PTB chamber, except for the PPAC that were normalized in the 1–10 MeV range. The inset shows the normalization to the PTB chamber.

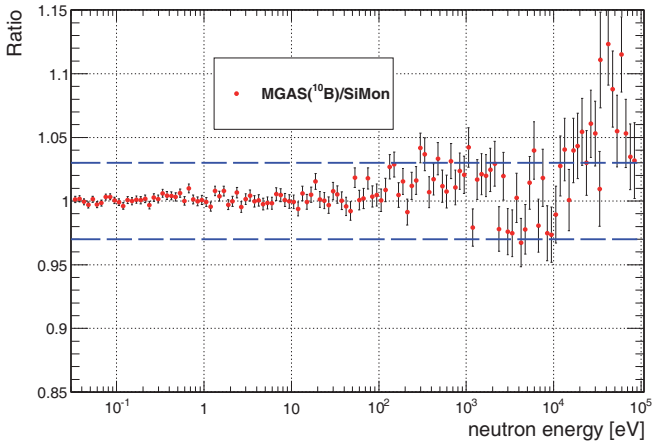

Fig. 7. Ratio of the fluxes measured with MGAS(^{10}B) and SiMon in the energy range 30 meV–100 keV. The blue dashed lines represent a deviation of 3%.

3.5 PPAC

Since PPACs are essentially insensitive to γ-radiation and the response of the anode signal is very fast, the time needed for the detector to recover after the so called γ-flash, *i.e.* the prompt signal caused by γ-rays and ultrarelativistic particles produced in the spallation target (see [7] for a detailed discussion), is small. This allows one to extend the measurement of the neutron flux up to 1 GeV neutron energy. In addition, the fission events were identified as coincidence signals in the anodes of two consecutive PPACs, rejecting most of the background produced by the α activity of the samples and by spallation reactions in the materials surrounding the samples. More details on the analysis procedure of this detector can be found in [22]. The efficiency of the device is around 50%, since the backing on one side of the sample limits the angular acceptance of the system to approximately 65 degrees. Up to a neutron energy of a few tens of keV, the efficiency is constant, while it increases at higher energy due to the variation in the fission fragment angular distribution in the laboratory system. In the present analysis, only the energy dependence of the efficiency was considered, rather than its absolute value. since the neutron flux measured with the PPACs is normalized to the PTB results between 1 and 10 MeV as shown below.

4 Results

Figure 6 shows the overall comparison of the neutron flux obtained with the four different systems, from near thermal to 1 GeV, after normalization to a common value at thermal neutron energy (the flux is expressed in units of lethargy and for the nominal proton pulse of $7 \cdot 10^{12}$ protons). The choice to normalize all results close to thermal energy (*i.e.* around 30 meV), where the cross sections of all involved reactions are either standard or, for the ^{235}U(n, f), known with an uncertainty of less than 0.5%, allows one to remove the systematic uncertainties related to the efficiency correction and to the areal density of the converter, which are independent of neutron energy and thus do not affect the shape of the neutron flux. Up to 1 eV, very good agreement is observed between the four detectors. Between 1 eV and 3 keV, good agreement is also found between the flux obtained with the SiMon and by MGAS(^{10}B) detectors, which show a smooth behavior. The large number of resonances in the ^{235}U(n, f) reaction in this energy region makes it difficult to extract the neutron flux from this reaction. Furthermore, a smoothed flux obtained from the MGAS(^{235}U) data shows that this reaction is not suited in the resonance region, most probably due to unreliable cross sections in the valleys, as already indicated in ref. [23]. Above 100 keV, a generally good agreement is observed between the PTB and MGAS(^{235}U) results while, as expected, the detectors based on the ^{6}Li and ^{10}B reactions are not very reliable because of angular anisotropy effects.

A more detailed comparison of the results was performed, in the energy range in which the involved cross sections are standard. Figure 7 shows the ratio between the flux extracted from the SiMon and MGAS(^{10}B) systems: below a few keV, where the results agree within 2%, while a difference of about 5% is observed above a few tens of keV, related to several absorption dips and to angular anisotropy corrections for both reactions. Based on the comparison, a weighted average of the two results was then used to extract an evaluated neutron flux from thermal energy to 100 keV, with the weights being purely the statistical errors.

It is interesting to compare this evaluated flux at low energy with the results based on the ^{235}U(n, f) reaction. Figure 8 shows that the agreement is slightly worse, although still within 2%. This is not surprising, considering that the ^{235}U(n,f) cross section is not standard in this energy region. Although a 2% agreement can still be considered very reasonable, it has not been judged

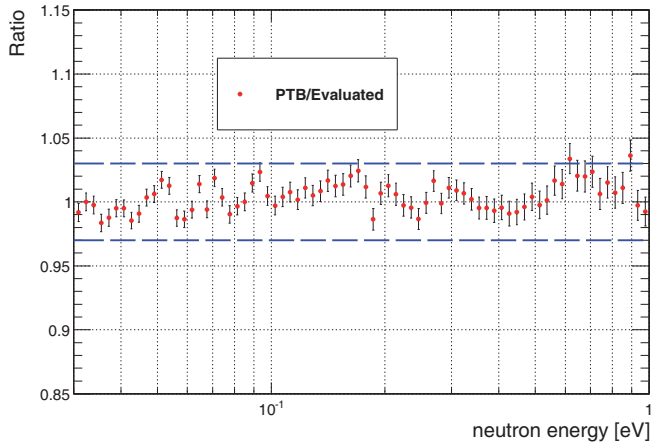

Fig. 8. Ratio of evaluated flux with the flux measured with PTB in the energy range 30 meV–1 eV. Blue dashed lines represent a deviation of 3%.

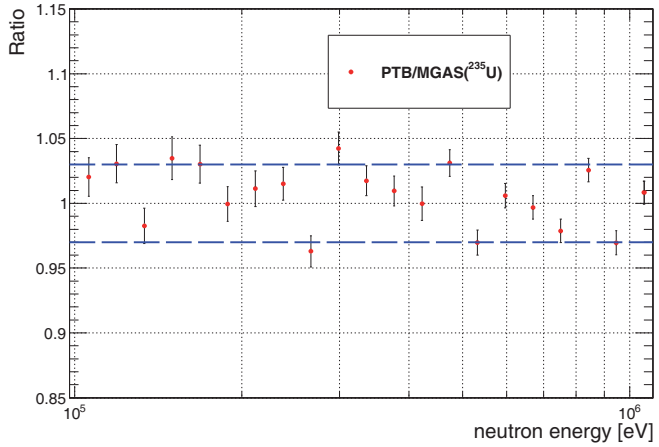

Fig. 9. Ratio of the fluxes measured with PTB and MGAS(^{235}U) in the energy range 100 keV–1 MeV. Blue dashed lines represent a deviation of 3%.

satisfactory if compared to the one between SiMon and MGAS(^{10}B) in the same energy range. Moreover, some structures can be observed in the ratio in fig. 8, indicating that the ^{235}U(n, f) cross section may indeed need some minor refinement between 100 meV and 1 eV.

In the range 100 keV–1 MeV a weighted average of PTB and MGAS(^{235}U) results based purely on the respective statistical errors, is used to evaluate the flux, since in this range the other two reactions are not cross section standards. Most importantly, the other two detectors in this energy range are heavily affected by issues related to the γ-flash and uncertain efficiency corrections. The ratio of the flux determined from the PTB and MGAS(^{235}U) in this range is shown in fig. 9. Between 1 and 10 MeV, only the PTB results are considered reliable and used for the evaluated flux, mainly because of the strong effect of the γ-flash on the MGAS(^{235}U) response. Finally, above 10 MeV, the only reliable data are those obtained from the PPAC detectors since this system is essentially insensitive to the prompt γ-rays and relativistic particles produced in the spallation target. Since the PPAC measurement was performed with the fission collimator, the results were normalized to those from PTB chamber in the energy region 1–10 MeV.

Table 3 indicates how the various results have been combined in the different energy ranges for obtaining the evaluated n_TOF neutron flux. The respective choices were made according to the energy ranges, where the various cross sections are established standards, as well as to the uncertainty of each result. A discussion of the final statistical and systematic uncertainty has been already presented in [7]. We recall here that the systematic uncertainties affecting the absolute value of the flux cancel out by the normalization relative to the PTB results. This does not hold, however, for the energy dependence of the flux. Two remaining sources of systematic uncertainty affect the energy dependence of the flux: anisotropies in the angular distribution of the reaction products and uncertainties in the cross sections, which in some cases may be larger than declared in the databases. The overall estimated systematic uncertainty is summarized in table 4. From thermal to 100 keV neutron energy, the systematic uncertainty was estimated on the basis of the comparison between the various results (see figs. 7 and 8), while at higher energy, where only the PTB or the PPAC systems were used, the reported values are the combination of the uncertainty of the reference cross sections ($\sim$ 1%) and of the corrections for dead-time and angular distribution effects. In particular, while the uncertainty related to dead-time corrections is below 1% even above 10 MeV, thanks to the fast response of the PPAC system, the correction for angular anysotropy, which reaches a maximum of 2.5% around 20 MeV, is based on low-accuracy data, so that a 1% uncertainty related to this correction has been assumed on the extracted flux.

The measurements described above were repeated at the beginning of each year, in 2009, 2010 and 2011. Figure 10 shows the evaluated flux for each of the three years. In 2009 normal water was used as moderator, while starting in 2010 borated water was used instead. The effect in this case is a strong reduction of the thermal peak. The small difference in the thermal region between 2010 and 2011 is related to a slight modification of the moderator circuit, which implies a controlled change of the ^{10}B concentration in the borated water. Above a few keV, the flux is equal for all three years, *i.e.* does not depend on the moderator liquid used. This is somewhat expected, because neutrons above a few keV are produced directly in the spallation process or undergo some moderation in the target itself. The constant behavior of the flux above a few keV, independently of the boron content, is confirmed by the simulations, and allows one to combine the results from several years to reduce the statistical errors. Another feature of the flux above a few keV is the presence of several dips, corresponding to resonances, mostly in the Al cross section, and therefore related to neutron absorption in the Al windows at the exit of the spallation target and at the entrance of the beam line.

Table 3. Summary of the detectors used in the evaluation of the n_TOF flux in different energy ranges up to 1 GeV. PTB^{th} indicates that at thermal energy the results of the PTB chamber have been used as reference to normalize all other results.

Energy range	30 meV–100 keV	100 keV–1 MeV	1–10 MeV	10 MeV–1 GeV
Detector used	SiMon	–	–	–
	MGAS(^{10}B)	–	–	–
	–	MGAS(^{235}U)	–	–
	PTB^{th}	PTB	PTB	–
	–	–	–	PPAC

Table 4. Overall estimated systematic uncertainty.

Energy range	Uncertainty
0.025 eV–100 eV	1%
100 eV–10 keV	2%
10 keV–100 keV	4–5%
100 keV–10 MeV	∼ 2%
10 MeV–1 GeV	∼ 3%

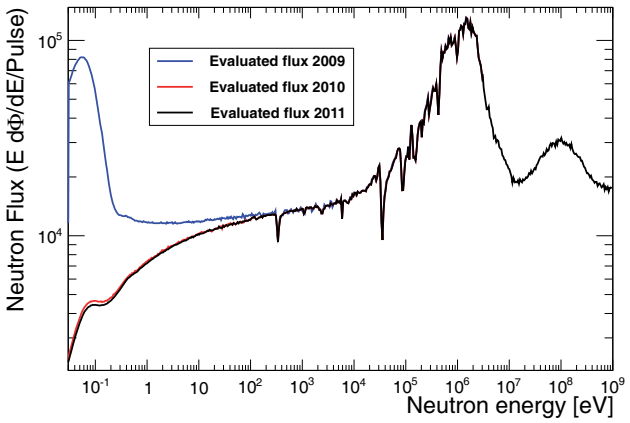

Fig. 10. Neutron flux at n_TOF for the campaigns 2009, 2010 and 2011 from thermal to 1 GeV neutron energy.

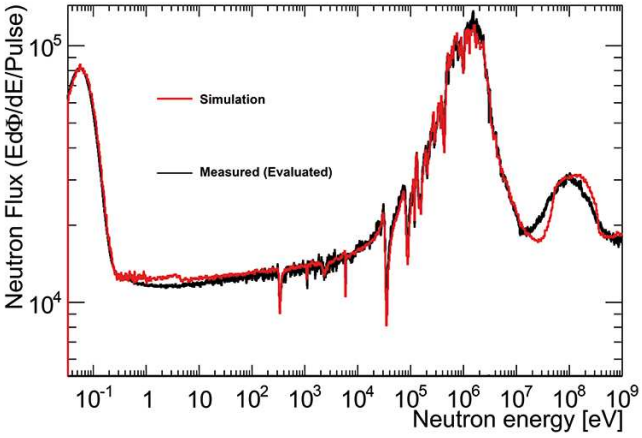

Fig. 11. Comparison of simulation and evaluated flux in the range 30 meV–1 GeV.

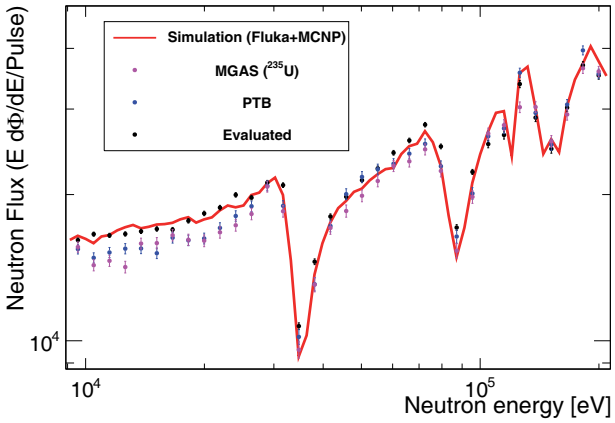

Fig. 12. Comparison of simulation, evaluated flux and results from detectors based on $^{235}U(n, f)$. In the range 10–30 keV a discrepancy can be observed between evaluated flux and simulation on the one hand, and PTB and MGAS(^{235}U) on the other hand.

4.1 Simulations

To complement and corroborate the results of the measurements, simulations of the neutron flux have been performed [7] by a combination of two Monte Carlo codes for neutron production and transport: FLUKA [24] and MCNPX. In particular, FLUKA is used to simulate the spallation process and neutron production at high energy, while MCNPX is subsequently used to simulate the moderation process inside the spallation target and moderator. For a consistent comparison with experimental data, the neutron energy is reconstructed from the simulated time of flight, assuming the effective flight path as described in [7].

The results of the simulations are in fair agreement with the experimental results in the whole energy range, except at very high energy as shown in fig. 11. In particular, very good agreement is found up to several MeV, even in the absorption dips. This confirms that geometrical details and effect of the materials were properly considered in the simulations. In turn, this observation provides a further confidence on the experimental results. Finally, essentially unlimited statistics can be obtained in the simulations for a more detailed description of the absorption dips.

4.2 The ^{235}U(n,f) cross section between 10 and 30 keV

In the analysis of the neutron flux extracted from the various detectors, an unexpected behavior was observed on the results based on the ^{235}U fission reaction, in the energy range between 10 and 30 keV. The results of both the PTB chamber and the MGAS(^{235}U) detectors agree with each other in this energy range but are lower, by 8–10%, relative to the flux measured by SiMon or MGAS(^{10}B). Figure 12 shows the comparison between the PTB and MGAS(^{235}U) results, on the one hand, and the evaluated and simulated flux, on the other hand. In this energy region, the ^{235}U fission cross section is not a standard, so that a perfect agreement is not expected. Nevertheless, it is generally believed that the maximum uncertainty on that cross section is around 1% (see ref. [9], which reports similar values). The results obtained at n_TOF seem to indicate, on the contrary, that there could be a problem in that energy region in current libraries, with the cross section possibly overestimated by much more than declared uncertainties. We recall that the cross sections used in the determination of the neutron flux were taken from the ENDF-B/VII.1 library [25], but similar results were obtained using the JENDL-4.0 library [26], which reports slightly different values. The difference observed between the evaluated flux and the one determined on the basis of the ^{235}U(n, f) reaction could have two possible explanations: either the systematic uncertainties in the evaluated flux obtained with the ^{6}Li and ^{10}B reactions are larger than expected due to the effect of the angular distributions or the ^{235}U(n, f) cross section in current libraries is overestimated in this energy region.

While at this stage the first possibility cannot be completely ruled out, the comparison with the simulations, also shown in fig. 12, provides further evidence for the second possibility. In the 10–30 keV energy region, in fact, remarkably good agreement is found between the measured and simulated neutron flux, and it seems unlikely that both results are systematically higher than expected, by the same amount. Nevertheless, a definite conclusion cannot be reached at this stage, and more dedicated measurements in this energy region are called for.

As a further remark, the present finding may help explaining a 10% discrepancy in the ^{235}U capture cross section recently observed in the same energy range in a measurement performed at Los Alamos Neutron Science Center by means of the ratio method, with a combined capture-fission apparatus (see [27] for details).

If confirmed, the anomaly observed in the present work may lead to a revision of the ^{235}U fission cross section in the 10-30 keV neutron energy range, a region of importance for the development of new nuclear systems based on fast neutrons.

5 Conclusions

The results of a series of measurements performed with the aim of determining the neutron flux at the n_TOF facility have been reported. In order to identify and minimize systematic effects and to cover the very wide energy range of the neutron beam, three different reactions and four different detection systems were used. The various results have been carefully compared and combined, yielding an evaluated flux to be used in cross sections measurements at n_TOF, in particular for capture reactions. An accuracy ranging between 1 and 5% has been achieved in the whole energy region, from thermal to approximately 1 GeV.

An anomaly in the flux obtained on the basis of the ^{235}U(n, f) reaction indicates that the cross section of this reaction between 10 and 30 keV may be overestimated by approximatively 8%, a value much higher compared with the systematic uncertainties claimed for the current data in the cross section libraries as well in standard compilations. Dedicated measurements specifically devoted to the investigation of this anomaly should be performed, and are planned at n_TOF for the next experimental campaign.

The authors are indebted to the national and international funding agencies that have supported the n_TOF Collaboration. This work is also supported by the European Commission with the FP7 project ANDES (FP7-249671). Furthermore, the measurements with the PTB detector would not have been possible without the support from the Physikalisch-Technische Bundesanstalt Institute, particularly from Ralf Nolte and Marita Mosconi who helped in installing and using the detector at n_TOF.

References

1. `https://ntof-exp.web.cern.ch/ntof-exp/`.
2. G. Wallerstein *et al.*, Rev. Mod. Phys. **69**, 995 (1997).
3. F. Käppeler, R. Gallino, S. Bisterzo, Wako Aoki, Rev. Mod. Phys. **83**, 157 (2011).
4. N. Colonna *et al.*, Energy Environ. Sci. **3**, 1910 (2010).
5. OECD/NEA WPEC Subgroup 26 Final Report, *Uncertainty and Target Accuracy Assessment for Innovative Systems Using Recent Covariance Data Evaluations*, `http://www.nea.fr/html/science/wpec/volume26`, NEA No. 6410 (2008).
6. E. Chiaveri *et al.*, J. Kor. Phys. Soc. **59**, 1620 (2011).
7. C. Guerrero *et al.*, Eur. Phys. J. A **49**, 27 (2013).
8. A.D. Carlson, Metrologia **48**, S328 (2011).
9. International Atomic Energy Agency, *International Evaluation of Neutron Cross-Section Standards* (Vienna, 2007).
10. S. Marrone *et al.*, Nucl. Instrum. Methods A **517**, 389 (2004).
11. I. Giomataris *et al.*, Nucl. Instrum. Methods A **376**, 29 (1996).
12. S. Andriamonje *et al.*, J. Kor. Phys. Soc. **59**, 1597 (2011).
13. D.B. Gayther, Metrologia **27**, 221 (1990).
14. C. Paradela *et al.*, Phys. Rev. C **82**, 034601 (2010).
15. D. Tarrío *et al.*, Phys. Rev. C **83**, 044620 (2011).
16. I. Giomataris, R. De Oliveira, *Method for fabricating an amplification gap of an avalanche particle detector*, Patent CEA-CERN, Application Number 09 290 825.0 (2009).
17. U. Abbondanno *et al.*, Nucl. Instrum. Methods A **538**, 692 (2005).
18. S. Agostinelli *et al.*, Nucl. Instrum. Methods A **506**, 250 (2003).
19. F.J. Hambsch, I. Ruskov, Nucl. Sci. Eng. **163**, 1 (2009).

20. G. Lorusso *et al.*, Nucl. Instrum. Methods A **532**, 622 (2004).
21. L.S. Waters *et al.*, AIP Conf. Proc. **896**, 81 (2007).
22. D. Tarrío, *Neutron-induced fission fragment angular distribution at CERN n_TOF: The Th-232 case*, PhD thesis (2012).
23. M. Calviani *et al.*, Phys. Rev. C **80**, 044604 (2009).
24. A. Ferrari *et al.*, *Fluka: A multi-particle transport code*, Technical Report CERN-2005-010, INFN/TC_05/11, SLAC-R-773 (2005).
25. M.B. Chadwick *et al.*, Nucl. Data Sheets **112**, 2887 (2011).
26. K. Shibata *et al.*, J. Nucl. Sci. Technol. **48**, 1 (2011).
27. M. Jandel *et al.*, Phys. Rev. Lett. **109**, 202506 (2012).